$\mathcal{L}_1$ Adaptive Manoeuvring Control of Unmanned High-speed Water Craft

Casper H. Svendsen [*] **Niels Ole Holck** [*] **Roberto Galeazzi** [*]
Mogens Blanke [*],[**]

[*] *Department of Electrical Engineering, Automation and Control
Group, Technical University of Denmark, Kgs. Lyngby, Denmark
(e-mail: {casper.h.svendsen, nielsoleholck}@gmail.com,
{rg, mb}@elektro.dtu.dk)*
[**] *Centre for Ships and Ocean Structures, Norwegian University of
Science and Technology, Trondheim, Norway*

Abstract: This work addresses the issue of designing an adaptive robust control system to govern the steering of a high speed unmanned personal watercraft (PWC) maintaining equal performance across the craft's envelope of operation. The maneuvering dynamics of a high speed PWC is presented and a strong variation over the envelope of operational conditions, including speed, is highlighted. The complexity of the nonlinear dynamics is overcome through identification of linear models at different speed regimes. A gray-box identification is conducted from full scale experiments and results in a four degrees-of-freedom surge-sway-yaw-roll model. An $\mathcal{L}_1$ adaptive autopilot is then designed, which allows to achieve fast adaption to system parameters' changes and robustness of the closed loop system.

Keywords: $\mathcal{L}_1$ adaptive control, Grey-box identification, LPV systems, Unmanned vehicles, High-speed maneuvering

1. INTRODUCTION

High-speed personal watercraft (PWC) are mostly used for recreational activities; however due to the inherent rapidity and agility, their use could be largely stretched to e.g. coast patrolling, surveillance of installation area, and search and rescue operation in harsh conditions. Safe and efficient performance of these tasks would require the possibility of operating those vehicles unmanned.

If unmanned navigation is to be achieved then seaworthiness must be guaranteed across a large range of operational conditions. High-speed planing craft are exposed to several stability problems, which arise as consequence of the large accelerations they can perform and the large speeds they can travel at. Dynamic stability issues like porpoising, large heel, bow diving, difficulty of course keeping (Dand, 1996; Blount and Codega, 1992) clearly address that the safety of the PWC and of its missions is tightly related to its manoeuvring capabilities. The manoeuvring dynamics of displaced vessels is generally described by 2 (sway-yaw) or 3 (surge-sway-yaw) degrees-of-freedom (DOF) models (Clarke and Horn, 1997; Blanke, 1981) where the heave, pitch and roll are neglected. Four degrees-of-freedom surge-sway-yaw-roll models have also been proposed by e.g. Son and Nomoto (1982); Blanke and Christensen (1993); Ross (2008), which aimed at investigating the coupling between steering and rolling. Although those models may present a certain level of complexity they have the advantage that their hydrodynamic derivatives – added masses and damping – are only function of the frequency of the excitation; further the assumption of calculating those parameters at zero frequency is commonly done (Fossen, 2011).

Completely different is the situation for high-speed crafts where the manoeuvring characteristics are influenced also by the vehicle's vertical dynamics. In particular Ikeda et al. (2000) showed through towing tank tests that the hydrodynamic forces and moments acting on a planing craft strongly depend on the running attitude (draft, trim, heel). This implies that the manoeuvring motions alter the craft's attitude, which in turn affects the manoeuvring characteristics. Therefore planing crafts would require 6 DOF models to fully describe their manoeuvring dynamics. Two distinct challenges stand out: the increased model complexity, and the dependence of the hydrodynamic derivatives on the running attitude. This implies an evident difficulty in establishing complete and reliable nonlinear models capable of describing the manoeuvring behaviour of a planing craft for a large range of operational conditions. As consequence clear limitations arise for the design of manoeuvring control system if equal performance is to be maintained throughout the operational range.

This paper proposes to model the manoeuvring characteristics of a PWC through the identification of a set of linear parameter varying (LPV) models around relatively close operating points. The manoeuvring dynamics is thus described as the transition among LTI systems through the parameter space. Grey-box identification is performed by exploiting several data set from full scale sea trials, where circular tests and zig-zag tests were carried out. The identification results in two major findings: a set of LPV systems that reliably describe the steering dynamics
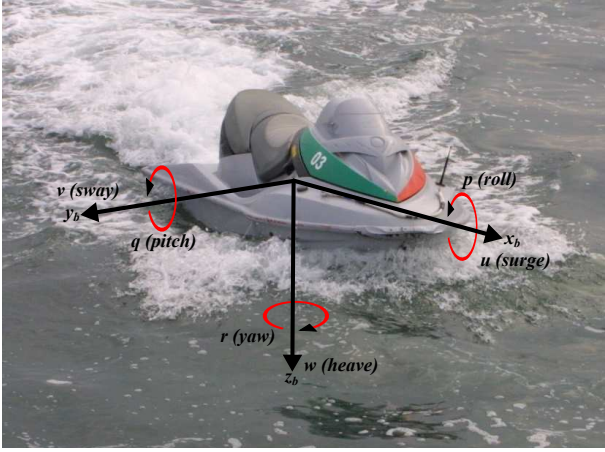
Fig. 1. Sea-Doo GTX 215 personal watercraft at sea.

within a large set of operational conditions, and the set of parameters that are mostly affected by changes in the running attitude together with their range of variation around nominal values.

The paper also looks into the problem of designing manoeuvring control systems, which are robust with respect to rapid and large changes of the craft's dynamics. By exploiting the knowledge about parameters variations gathered through an identification procedure, an adaptive manoeuvring controller is designed by means of $\mathcal{L}_1$ adaptive control theory (Hovakimyan and Cao, 2010). The $\mathcal{L}_1$ adaptive autopilot is shown to guarantee both robustness and stability of the closed loop system over a large envelope of operational conditions. With only one reported study, by Breu and Fossen (2011), in the application of $\mathcal{L}_1$ theory to ship control, the application to this domain is quite novel.

2. SYSTEM SETUP

The vehicle is a modified version of a Sea-Doo GTX 215 personal watercraft (see Fig. 1), where servos have been added to control both the throttle and the azimuth angle of the propeller propulsion. A radio receiver is installed to have remote control of the vehicle. Vehicle dimensions and specifications are listed in Table 1.

The servos controlling the throttle and the steering are driven by pulse width modulated (PWM) signals. Feedback about the position of the servos is not available. The gas handle servo controls the air intake of the engine, which has a built-in "intelligent throttle control" functionality responsible of controlling the throttle based on air intake and the current throttle command. There is no direct control of the throttle. Steering of the vehicle is achieved by directing the propulsion angle relative to the vessel's centre line, which in turn determines a moment around the Z-axis. The maximum angular deflection δ of the waterjet is 15° to either side.

The vehicle is equipped with navigation sensors including GPS, 3-axis magnetometer, 3-axis accelerometer, and 3-axis rate gyro.

Table 1. Sea-Doo GTX 215 specifications

Quantity	Measure
Nominal length (measured)	3.25 m
Width	1.22 m
Dry weight	388 kg
Engine max power	158 kW

3. PWC MANOEUVRING DYNAMICS

The manoeuvring dynamics of a PWC is presented by using a 4 DOF surge-sway-yaw-roll model first introduced by Son and Nomoto (1982) (gravity centre based), as symmetry centre based in Blanke and Christensen (1993) and widely used, see e.g. Perez and Blanke (2012) and references herein.

Define $\boldsymbol{\eta} \triangleq [x, y, \phi, \theta]^{\mathrm{T}} \in \mathbb{R}^2 \times \mathcal{S}^2$ as the vector of generalised coordinates in an Earth-fixed frame; $\boldsymbol{\nu} \triangleq [u, v, p, r]^{\mathrm{T}} \in \mathbb{R}^4$ as the vector of generalised linear and angular velocities in the body-fixed frame; $\mathbf{r}_g \triangleq [0, 0, z_g]^{\mathrm{T}} \in \mathbb{R}^3$ as the position of the centre of gravity w.r.t. the origin (centre of symmetry) of the body-fixed frame. Adopting the matrix formulation introduced by Fossen (1991, 2011) the manoeuvring dynamics in the body-fixed frame is given by

$$\mathbf{M}\dot{\boldsymbol{\nu}} + (\mathbf{C}(\boldsymbol{\nu}) + \mathbf{D}(\boldsymbol{\nu}))\boldsymbol{\nu} + \mathbf{g}(\boldsymbol{\eta}) = \boldsymbol{\tau}_c + \tau_e \qquad (1)$$

where $\mathbf{M} = \mathbf{M}^{\mathrm{T}} > 0$ is the vehicle inertia matrix, which includes the rigid body and added mass-inertia

$$\mathbf{M} = \begin{bmatrix} m - X_{\dot{u}} & 0 & 0 & 0 \\ 0 & m - Y_{\dot{v}} & -mz_g - Y_{\dot{p}} & -Y_{\dot{r}} \\ 0 & -mz_g - K_{\dot{v}} & I_x - K_{\dot{p}} & 0 \\ 0 & -N_{\dot{v}} & 0 & I_z - N_{\dot{r}} \end{bmatrix},$$

$\mathbf{C}(\boldsymbol{\nu})$ is the Coriolis-centripetal matrix

$$\mathbf{C}(\boldsymbol{\nu}) = \begin{bmatrix} 0 & 0 & mz_g r & -mv \\ 0 & 0 & 0 & mu \\ -mz_g r & 0 & 0 & 0 \\ mv & -mu & 0 & 0 \end{bmatrix}$$

$$+ \begin{bmatrix} 0 & 0 & 0 & Y_{\dot{v}}v + Y_{\dot{r}}r + Y_{\dot{p}}p \\ 0 & 0 & 0 & X_{\dot{u}}u \\ 0 & 0 & 0 & 0 \\ -Y_{\dot{v}}v - Y_{\dot{r}}r - Y_{\dot{p}}p & X_{\dot{u}}u & 0 & 0 \end{bmatrix},$$

$\mathbf{D}(\boldsymbol{\nu}) > 0 \; \forall \; \boldsymbol{\nu} \in \mathbb{R}^4$ is the linear (potential and viscous) plus quadratic damping matrix

$$\mathbf{D}(\boldsymbol{\nu}) = - \begin{bmatrix} X_u & 0 & 0 & 0 \\ 0 & Y_v & 0 & Y_r \\ 0 & 0 & K_p & 0 \\ 0 & N_v & 0 & N_r \end{bmatrix}$$
$$- \begin{bmatrix} X_{|u|u}|u| & 0 & 0 & 0 \\ 0 & Y_{|v|v}|v| & 0 & 0 \\ 0 & 0 & K_{|p|p}|p| & 0 \\ 0 & 0 & 0 & N_{|r|r}|r| \end{bmatrix},$$

and $\mathbf{g}(\boldsymbol{\eta})$ is the vector of gravitational and buoyancy forces and moments

$$\mathbf{g}(\boldsymbol{\eta}) = \begin{bmatrix} 0 \\ 0 \\ \rho g \nabla \overline{\mathrm{GM}}_{\mathrm{T}} \phi \\ 0 \end{bmatrix}$$

with ρ being the water density, g the acceleration of gravity constant, ∇ the displacement of the vehicle, and $\overline{\mathrm{GM}}_{\mathrm{T}}$ the transverse metacentric height in calm water. $\boldsymbol{\tau}_c$ is

the control inputs vector, and $\boldsymbol{\tau_e}$ is the environmental disturbances vector, which includes forces and moments due to wind, waves and currents.

The identification of the manoeuvring dynamics is performed by using full scale motion data collected during circular tests and zig-zag tests run in "calm" water conditions. Only vehicle's motion data are available, which precludes the possibility of directly identifying the coefficients of $\mathbf{M}$, $\mathbf{D}(\boldsymbol{\nu})$, $\mathbf{C}(\boldsymbol{\nu})$, and of the vector $\mathbf{g}(\boldsymbol{\eta})$, as this would also require measurements of the forces and moments acting on the vehicle. Therefore, the identification aims at providing estimates of the parameters of the following model where $\boldsymbol{\tau}_e = \mathbf{0}$

$$\dot{\boldsymbol{\nu}} = -\mathbf{M}^{-1}\left[(\mathbf{C}(\boldsymbol{\nu}) + \mathbf{D}(\boldsymbol{\nu}))\boldsymbol{\nu} + \mathbf{g}(\boldsymbol{\eta})\right] + \mathbf{M}^{-1}\boldsymbol{\tau}_c. \quad (2)$$

Identification from full scale measurements is divided into two parts: the surge dynamics is first considered independently; then the steering plus roll dynamics is identified.

3.1 Identification of Surge Dynamics

Theoretically, the surge dynamics of the personal watercraft has the form

$$(m - X_{\dot{u}})\dot{u} - (X_u + X_{|u|u}|u|)u + (mz_g + Y_{\dot{p}})pr$$
$$- (m - Y_{\dot{v}})vr + Y_{\dot{r}}r^2 = \tau_u \quad (3)$$

where $\tau_u = (1 - t)T(n, u_p)$ is the effective thrust with $T(n, u_p)$ being the thrust generated by the propeller, and t the thrust deduction. The propeller thrust is a function of the shaft speed and of the axial flow velocity in the propeller disc (Blanke et al., 2000). However, the system set-up measures neither the propeller thrust T or the axial flow velocity, and provides no direct control of the shaft speed. Only the handle command h is known.

The handle command h is a real value variable taking values in $h \in [1, 7] \subset \mathbb{R}$, where 1 is the idle state of the engine, and 7 is full throttle. When remotely controlled, the minimum handle command gives an idle power P_s that will give the WPG a $U_{\min,ss} = 2$ m/s forward speed. Propeller thrust is hence considered a function of the surge speed and the handle command

$$T \triangleq T(u; h) \quad (4)$$

and an empirical relation needs be determined to describes how T, u and h are related. To achieve this the following steps have been undertaken:

- estimate resistance coefficients X_u, $X_{u|u|}$ surge data in response to steps in the handle command
- determine steady state relations between T and u.

From (2) the surge dynamics reads

$$\dot{u} = \alpha_1 u + \alpha_2 u|u| + \alpha_3 vr + \alpha_4 pr + \alpha_5 r^2 + \tilde{\tau}_u \quad (5)$$

where $\alpha_1 = X_u/(m - X_{\dot{u}})$; $\alpha_2 = X_{u|u|}/(m - X_{\dot{u}})$; $\alpha_3 = -(m - Y_{\dot{v}})/(m - X_{\dot{u}})$; $\alpha_4 = (mz_g + Y_{\dot{p}})/(m - X_{\dot{u}})$; $\alpha_5 = Y_{\dot{r}}r^2/(m - X_{\dot{u}})$; $\tilde{\tau}_u = T(u; h)/(m - X_{\dot{u}})$.

When the vehicle moves at a straight course in calm water, its dynamics is dominated by the propeller thrust and by the water resistance; hence the contribution of the forces due to sway, roll and yaw can be neglected. Thus (5) simplifies to

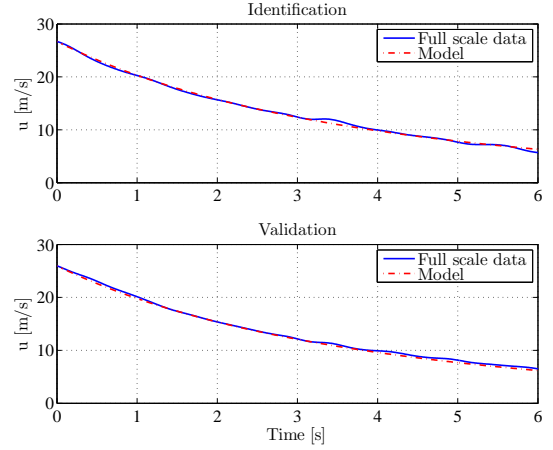$$\dot{u} = \alpha_1 u + \alpha_2 u|u| + \tilde{\tau}_u. \quad (6)$$

Fig. 2. Throttle steps: $h = 4 \to 1, h = 7 \to 1, \alpha_1 = -0.1926, \alpha_2 = -0.0035$.

Now assume the vehicle is moving at constant surge speed $u(t_0) = \bar{u}$, and we let the propeller thrust step to zero $\tilde{\tau}_u = 0$. This instant is denoted $t = t_0$. According to (6) the surge velocity will decay under the action of the friction forces at an exponential rate larger than $-1/\alpha_1$, i.e.

$$u(t) \leq \bar{u}e^{-\alpha_1 t}, \quad \forall\, t > t_0. \quad (7)$$

In practice, the propeller thrust can not reach zero through the handle command, but only reach the idle mode where a minimum thrust $\tilde{\tau}_{u,\min}$ corresponds to vehicle forward speed $U_{\min}$. However it is legitimate to assume that when switching the handle command from a certain value $h = \bar{h} \in [2, 7]$ to the idle mode ($h = 1$) the frictional forces will overcome the minimum thrust delivered by the propeller, and hence (7) is a good approximation of the surge velocity behaviour. The coefficients α_1 and α_2 can then be estimated through a standard nonlinear least-square method (Ljung, 1999) applied to the data set $[\dot{u}_{\text{acc}}^{\text{T}}, u_{\text{acc}}^{\text{T}}]$. Figure 2 shows the comparison between the full scale surge data and the response produced by the identified surge dynamics, both in identification and in validation. The response of the identified model matches very well the full scale data, confirming the validity of our assumption.

Impeller thrust in a steady state can be calculated from the estimated coefficients. When the vehicle is on a straight course at constant speed, the thrust and resistance are in balance

$$\dot{u} = 0 \Rightarrow \tilde{\tau}_{u,ss} = \alpha_1 u_{ss} + \alpha_2 u_{ss}|u_{ss}| \quad (8)$$

where u_{ss} is the steady state surge velocity and $\tilde{\tau}_u$ the thrust.

From a control prospective, the system set up does not allow to directly command a certain thrust, but through the handle command signal it is possible to set a certain shaft power Π_s, which in turn is related to the propeller thrust by

$$\Pi_s = \tilde{\tau}_u u. \quad (9)$$

An empirical formula of Π_s as a function of the handle command can be constructed from measured data at steady state

$$\Pi_s(h) = \begin{cases} m_1 h + q_1 & \text{if } 1 \leq h < 2 \\ s_1 h^2 + s_2 h + s_3 & \text{if } 2 \leq h < 4 \\ m_2 h + q_2 & \text{if } 4 \leq h \leq 7 \end{cases} \quad (10)$$

Table 2. Coefficients of Π_s

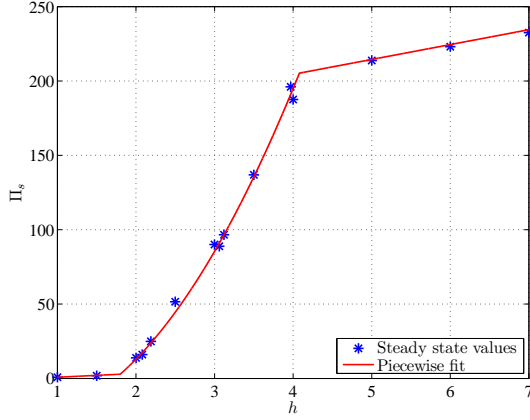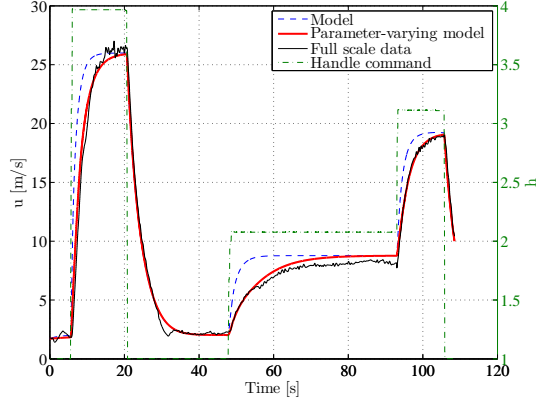|	Coefficients						
	m_1	m_2	q_1	q_2	s_0	s_1	s_2
Value	12.10	10.00	-11.30	164.5	-21.1	-20.0	18.5

Fig. 3. Empirical relation between the handle command h and the shaft power Π_s.

Fig. 4. Validation of the surge model against full scale data.

where the numerical values of the slopes m_i, the y-intercepts q_i, and the coefficients s_i are reported in Table 2 The handle command to shaft power relation is split into 3 regions (see Fig. 3): first a linear region, then a quadratic region, and last a linear region. With $\Pi_s(h)$ being available it is then possible to estimate the propeller thrust for any handle command

$$\tilde{\tau}_u(u;h) = \frac{\Pi_s(h)}{u}. \qquad (11)$$

The validity of the identified model was tested against full scale data, as shown in Fig. 4 where four consecutive steps were commanded. The identified surge dynamics (dashed red line) is accurately following the real dynamics when the throttle commands a negative step, as between 30 and 50 seconds. However, when positive step changes are commanded, the model rise time is smaller than that of the real system, which points at an estimate of the parameters α_1 and α_2 larger than the real values. This could be caused by differences in the intercepted waterplane area between the acceleration and the deceleration phases. By allowing the rate of change to be scaled, the time constant can be altered. The scaling factor is calculated as $\frac{u}{28}$ but limited to the interval $[0.2, 1]$. Also a rate limit on the handle

Table 3. Surge dynamics estimated coefficients

Coefficient	Value	Std. Dev.
α_1	-0.1926	4%
α_2	-0.0035	13%
α_3	+5.032	1%

command is added, to simulate the time it takes for the servo to adjust to a new position. The modified surge dynamics along a straight line course reads

$$\dot{u} = \kappa(\alpha_1 u + \alpha_2 u|u| + \tilde{\tau}_u), \quad \kappa \in [0.2, 1] \qquad (12)$$

When turning manoeuvres are considered the effect of centripetal forces is to be taken into account, and the coefficients α_3, α_4, and α_5 are to be identified. The coefficient α_3 has a dominant contribution to the surge dynamics if compared to α_4 and α_5. In fact, α_4 eventually affects the surge motion only at the beginning and at the end of a turn when roll rate p is different from zero. At the same time the coefficient α_5 can be neglected if we assume a symmetric hull. Hence by looking at steady state conditions during the circular tests the coefficient α_3 is found to be equal to 5.02.

Summarising the nonlinear dynamics, surge is given by

$$\dot{u} = \kappa(\alpha_1 u + \alpha_2 u|u| + \alpha_3 vr + \tilde{\tau}_u) \qquad (13)$$

where the estimated value of the coefficients with their standard deviations are shown in Table 3.

3.2 Steering Dynamics Identification

The steering dynamics is identified by fitting a linearised 3-DOF sway-roll-yaw model against full scale data gathered during circular tests and zig-zag tests.

Let define the state vector $\mathbf{x} \triangleq [u, p, r, \phi, \psi]^T$, the input vector $\bar{\tau} \triangleq [\tau_{v\delta}, \tau_{p\delta}, \tau_{r\delta}]^T$, and let assume that the ship forward speed $U \approx u$ – i.e. $u \gg v$. The structure of the linear model to be identified is then obtained by linearising (2) around the operating point $\mathbf{x}_0 = [U_0, 0, 0, 0, 0]^T$, which gives

$$\dot{\mathbf{x}} = \begin{bmatrix} \overline{\mathbf{M}}^{-1} & \mathbf{0} \\ \mathbf{0} & \mathbf{I}_{2\times2} \end{bmatrix} \left. \frac{\partial \mathbf{f}(\mathbf{x})}{\partial \mathbf{x}} \right|_{\mathbf{x}_0} + \begin{bmatrix} \overline{\mathbf{M}}^{-1} \\ \mathbf{0}_{1\times3} \\ \mathbf{0}_{1\times3} \end{bmatrix} \bar{\tau}$$

$$= \begin{bmatrix} a_1 & a_2 & a_3 & a_4 & 0 \\ a_5 & a_6 & a_7 & a_8 & 0 \\ a_9 & a_{10} & a_{11} & 0 & 0 \\ 0 & 1 & 0 & 0 & 0 \\ 0 & 0 & 1 & 0 & 0 \end{bmatrix} \mathbf{x} + \begin{bmatrix} b_1 \\ b_2 \\ b_3 \\ 0 \\ 0 \end{bmatrix} \delta \qquad (14)$$

where $\overline{\mathbf{M}} = \mathbf{M}_{[2:4,2:4]}$, $\mathbf{f}(\mathbf{x}) : \mathbb{R}^5 \to \mathbb{R}^5$ is the vector of the hydrodynamic and centripetal forces/moments acting on sway, roll and yaw.

Since no prior knowledge of the hydrostatic and hydrodynamic coefficients is available a first estimation of the parameters (a_i, b_j) is obtained through black box identification. At this point only the link between velocities and accelerations is considered, hence the coefficients a_4 and a_8 related to the action of the roll restoring moment on the sway and roll dynamics are neglected.

The parameters found through the black box identification are then used as initial guess in the further grey box identification. In setting up the grey box model some
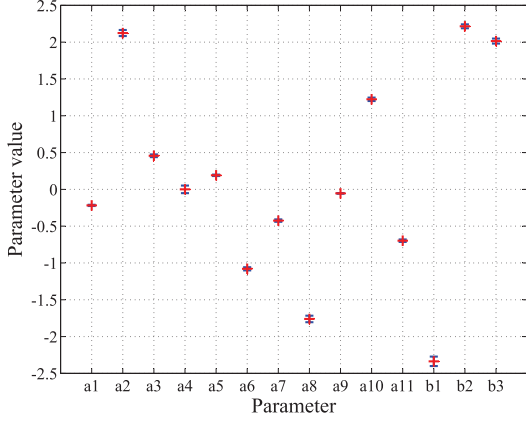
Fig. 5. Estimated parameters (red +) and their standard deviations (1 σ) shown by horizontal bars (blue -).

insight gained through the physical modelling is exploited. The parameters a_1, a_6 and a_{11}, are related to the sway, roll and yaw damping coefficients, therefore these parameters must be negative. The coefficient a_8 related to the roll restoring moment must also be negative in order for the vehicle to return to the upright position after a roll angle has been induced. The input gain b_1 relates the deflection of the propulsion direction to sway velocity, and because sway is defined positive starboard and the deflection is defined positive for a right turn then b_1 must be negative. The input gain b_2 relates the deflection of the propulsion direction to roll rate, and because roll rate is defined positive clockwise then b_2 must be positive. The input gain b_3 relates the deflection of the propulsion direction to yaw rate, and because yaw rate is defined positive clockwise then b_3 must be positive. The grey box model identified under the former constraints is

$$\dot{\mathbf{x}}(t) = \begin{bmatrix} -0.218 & 2.10 & 0.443 & -0.0157 & 0 \\ 0.184 & -1.06 & -0.433 & -1.74 & 0 \\ -0.0526 & 1.22 & -0.697 & 0 & 0 \\ 0 & 1 & 0 & 0 & 0 \\ 0 & 0 & 1 & 0 & 0 \end{bmatrix} \mathbf{x}(t)$$
$$+ \begin{bmatrix} -2.29 \\ 2.21 \\ 2.01 \\ 0 \\ 0 \end{bmatrix} \delta(t) \qquad (15)$$

and the uncertainty on the parameters estimation is shown in Fig. 5. Note that due to the large uncertainty the parameter a_4 is sign undetermined; therefore its contribution to the sway dynamics is discarded, i.e. $a_4 = 0$.

The identified model is validated against full scale data of a 15-90 zig-zag test, as shown in Fig. 6. The sway and yaw dynamics are well identified, whereas the roll rate is rather poorly fit due to the natural inadequacy of linear systems to model dynamics higher than first order. However the high frequency content is filtered out by the integral action, which provides a well fitted roll angle. Moreover, the zig-zag test shows that the vehicles dynamics is not symmetrical: whenever the vehicle is performing a right turn a small overshoot in the yaw rate can be noticed, which is not present when the vehicle turns left. However, there is no attempt to further model this discrepancies
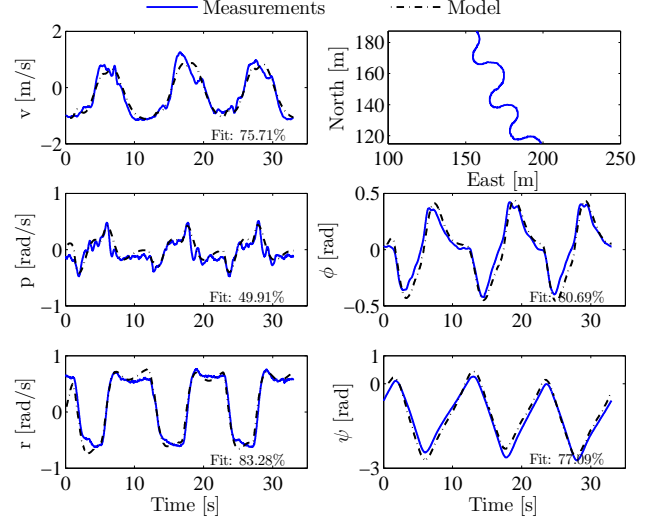

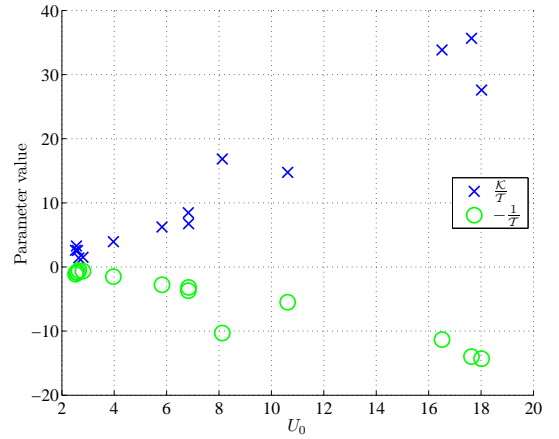Fig. 6. Grey box model validation: 15-90 zig-zag test.

Fig. 7. Forward speed dependency of the Nomoto model parameters for the personal watercraft.

since the $\mathcal{L}_1$ manoeuvring controller is expected to handle them.

LPV Yaw Model From the manoeuvring control prospective only the yaw dynamics is of interest; therefore (14) is reduced to a second order system. Let define the state vector $\mathbf{x}_1 \triangleq [r, \psi]^{\mathrm{T}}$, then the yaw dynamics simplifies to

$$\dot{\mathbf{x}}_1 = \begin{bmatrix} -\dfrac{1}{\tau} & 0 \\ 1 & 0 \end{bmatrix} \mathbf{x}_1 + \begin{bmatrix} \dfrac{\kappa}{\tau} \\ 0 \end{bmatrix} \delta \Rightarrow \frac{r}{\delta}(s) = \frac{\kappa}{1 + s\tau} \qquad (16)$$

that is the first order Nomoto model (Nomoto et al., 1957), where $\tau = (I_z - N_{\dot{r}})/N_r$ is the time constant and $\kappa = N_\delta/N_r$ is the input gain.

The validity of the Nomoto model is restrained to constant ship forward speed and to small deflections of the propulsion direction; hence its parameters κ/τ, and $-1/\tau$ are well known to be speed dependent. This is obviously confirmed by estimating those parameters for circular tests run at increasing forward speed, as shown in Fig. 7.

4. $\mathcal{L}_1$ MANOEUVRING CONTROL

The identification of the manoeuvring dynamics pointed out that both surge and steering are strongly dependent on the vehicle running attitude. In particular the ship forward speed U has a substantial influence on the steering characteristics, and the surge dynamics shows different behaviours in response to large positive and negative accelerations. Moreover constraining the modelling of the steering dynamics on the horizontal plane naturally excludes the influence of the motions in the vertical plane on yaw, which is known to be relevant for planing hulls (Ikeda et al., 2000). This large and fast variability of the manoeuvring characteristics calls in for the $\mathcal{L}_1$ adaptive control scheme (Hovakimyan and Cao, 2010), which can quickly compensate for uncertain and unmodelled dynamics still guaranteeing the robustness and stability of the closed loop system.

4.1 $\mathcal{L}_1$ Adaptive Cruise Control

The cruise control is achieved through the design of an $\mathcal{L}_1$ adaptive controller, which determines the thrust $\tilde{\tau}_u$ needed to follow the desired speed profile.

In agreement with the $\mathcal{L}_1$ adaptive control framework the surge dynamics (12) is reformulated as

$$\dot{u} = A_{m,u}u + (\omega_u\tilde{\tau}_u + g(t,u) + \sigma_u) \quad (17)$$
$$y_1 = u \quad (18)$$

where $A_{m,u} = \alpha_{\text{des}} \in \mathbb{R}^-$ is the desired exponentially stable surge dynamics, $\omega_u = \kappa(t) \in R^+$ is the unknown control input gain with known sign, $g(t,u) = (\alpha_1(t) + \alpha_2(t)|u|)u - \alpha_{\text{des}}u$ is an unknown nonlinear mapping continuous in its arguments, and $\sigma_u = \alpha_3(t)vr$ is a uniformly rate bounded unknown input disturbance. Further, $g(t,0)$ is uniformly bounded and its partial derivatives are piecewise continuous and semiglobally uniformly bounded.

The $\mathcal{L}_1$ adaptive cruise controller consists of three main subsystems (Hovakimyan and Cao, 2010):

- *state predictor* which provides the estimate of the surge speed u

$$\dot{\hat{u}} = A_{m,u}\hat{u} + \left(\hat{\omega}_u\tilde{\tau}_u + \hat{\theta}_u\,\|u\|_\infty + \hat{\sigma}_u\right),\ \hat{u} = u_0 \quad (19)$$

$$\hat{y}_1 = \hat{u} \quad (20)$$

- *parameter estimator* which provides the adaptive estimates of $\hat{\omega}_u$, $\hat{\theta}_u$ and $\hat{\sigma}$ according to

$$\dot{\hat{\theta}}_u = \Gamma_u\text{Proj}\left(\hat{\theta}_u, -\tilde{u}P_u\,\|u\|_\infty\right),\ \hat{\theta}_u(0) = \hat{\theta}_{u,0} \quad (21)$$

$$\dot{\hat{\sigma}}_u = \Gamma_u\text{Proj}\left(\hat{\sigma}_u, -\tilde{u}P_u\right),\ \hat{\sigma}_u(0) = \hat{\sigma}_{u,0} \quad (22)$$

$$\dot{\hat{\omega}}_u = \Gamma_u\text{Proj}\left(\hat{\omega}_u, -\tilde{u}P_u\tilde{\tau}_u\right),\ \hat{\omega}_u(0) = \hat{\omega}_{u,0} \quad (23)$$

where $\tilde{u} = \hat{u} - u$; $\Gamma_u \in \mathbb{R}^+$ is the adaptation gain, and $P_u > 0$ is the solution of the Lyapunov equation $A_{m,u}^{\text{T}}P_u + P_uA_{m,u} = -Q_u$ for an arbitrary $Q_u > 0$. The projection operator $\text{Proj}(\cdot)$ guarantees that the estimates are bounded.

- *controller* which commands the propeller thrust $\tilde{\tau}_u$ according to

$$\tilde{\tau}_u(s) = -k_uD_u(s)\left(\hat{\eta}_u(s) - k_{g,u}u_{\text{ref}}(s)\right) \quad (24)$$
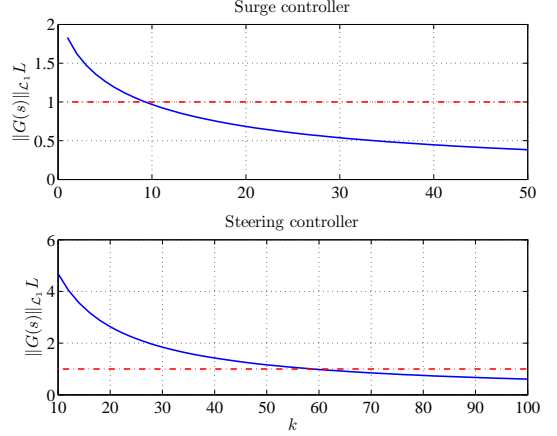

Fig. 8. $\|G_u(s)\|_{\mathcal{L}_1}L_u$ as a function of k_u.

where $\hat{\eta}_u(s)$ and $u_{\text{ref}}(s)$ are the Laplace transforms of $\hat{\eta}_u = \hat{\omega}_u\tilde{\tau}_u + \hat{\theta}_u\,\|u\|_\infty + \hat{\sigma}_u$ and of the reference surge speed, respectively. Setting the filter $D_u(s) = 1/s$ yields the low-pass filter $C(s) = \frac{\omega_uk_u}{s+\omega_uk_u}$, whose cutoff frequency is determined by the controller gain k_u. The feedforward gain $k_{g,u} = -1/\alpha_{\text{des}}$ guarantees reference tracking and zero steady state error for step changes of u_{ref}.

Design Specification The closed loop system is desired to have 95% settling time $t_{s,95} = 2.14\,\text{s}$; hence the eigenvalue of the desired dynamics has been chosen as $\alpha_{\text{des}} = -1.4$.

The implementation of the adaptation laws relies on the following bounded sets

- $\theta \in \Theta = [0.2025, 1.7716]$
- $\omega \in \Omega_0 = [0.1, 2.0]$
- $|\sigma_u| \le \Delta_{u,0} = 23.17, \forall\, t \ge 0$

To guarantee the robustness of the closed loop surge dynamics the $\mathcal{L}_1$-norm condition (Hovakimyan and Cao, 2010) must be satisfied

$$\|G_u(s)\|_{\mathcal{L}_1} < \frac{\rho_r - \|H_u(s)C_u(s)k_{g,u}\|_{\mathcal{L}_1}\|u_{\text{ref}}\|_{\mathcal{L}_\infty} - \rho_{in}}{L_u\rho_r + B} \quad (25)$$

where

$$G_u(s) = H_u(s)(1 - C_u(s))$$
$$H_u(s) = (s - \alpha_{\text{des}})^{-1}$$

and ρ_r, ρ_{in} defined as in (Hovakimyan and Cao, 2010). Figure 8 (top plot) shows a numerical evaluation of condition (25) for increasing value of the filter bandwidth k_u. It can be seen that for $k_u > 12.2$ the $\mathcal{L}_1$-norm condition is fulfilled,; however a larger bandwidth has been chosen for achieving greater disturbance rejection by setting $k_u = 35.0$. Moreover, the adaptation gain Γ_u is set to 10^4.

4.2 $\mathcal{L}_1$ Adaptive Steering Control

The control of the heading angle ψ is achieved through the design of a second $\mathcal{L}_1$ adaptive controller, which determines the deflection angle δ of the waterjet engine.

Under the assumption that pitch and roll angles are small – i.e. $\dot{\psi} \approx r$ – the yaw dynamics is reformulated in terms of the heading angle error. This averts that the controller

reacts differently depending on the sailing direction. Let define the heading error as $\psi_e = \psi_{\text{ref}} - \psi$, with $\psi_e \in [-\pi, \pi]$ and ψ_{ref} a constant reference heading, then the yaw dynamics reads

$$\begin{bmatrix} \dot{\psi}_e \\ \dot{r} \end{bmatrix} = \begin{bmatrix} 0 & -1 \\ 0 & \gamma_1 \end{bmatrix} \begin{bmatrix} \psi_e \\ r \end{bmatrix} + \begin{bmatrix} 0 \\ \gamma_2 \end{bmatrix} \delta \tag{26}$$

where $\gamma_1 = -1/\tau$ and $\gamma_2 = \kappa/\tau$.

Define the state vector as $\mathbf{x}_h \triangleq [\psi_e, r]^{\text{T}}$, and the input $u \triangleq \delta$. Then the steering dynamics (26) can be reformulated as

$$\dot{\mathbf{x}}_h = \mathbf{A}_{m,h}\mathbf{x}_h + \mathbf{b}_h \left(\omega_h \delta + \boldsymbol{\theta}_h^{\text{T}}\mathbf{x}_h + \sigma_h \right) \tag{27}$$

$$y_2 = \mathbf{c}_h^{\text{T}}\mathbf{x}_h \tag{28}$$

where $\mathbf{A}_{m,h}$ is the desired closed loop dynamics; $\mathbf{b}_h$ and $\mathbf{c}_h$ are known constant input and output vectors; $\omega_h \in \mathbb{R}^+$ is the unknown control input gain with known sign; $\boldsymbol{\theta}_h$ is the uniformly bounded and rate bounded unknown parameter vector; σ_h is the uniformly bounded and rate bounded unknown disturbance. For the system at hand the former quantities are given by

$$\mathbf{A}_{m,h} = \begin{bmatrix} 0 & -1 \\ a_1 & a_2 \end{bmatrix}, \quad \mathbf{b}_h = \begin{bmatrix} 0 \\ 1 \end{bmatrix}, \quad \mathbf{c}_h = \begin{bmatrix} 1 \\ 0 \end{bmatrix}$$

$$\boldsymbol{\theta}_h = \begin{bmatrix} -a_1 \\ -a_2 - \dfrac{1}{\tau} \end{bmatrix} \quad \omega_h = \frac{\kappa}{\tau}.$$

The $\mathcal{L}_1$ adaptive steering controller consists of the following subsystems:

- *state predictor* which provides the estimates of ψ_e and of r according to

$$\dot{\hat{\mathbf{x}}}_h = \mathbf{A}_{m,h}\hat{\mathbf{x}}_h + \mathbf{b}_h \left(\hat{\omega}_h \delta + \hat{\boldsymbol{\theta}}_h^{\text{T}}\mathbf{x}_h + \hat{\sigma}_h \right) \tag{29}$$

$$\hat{y}_2 = \mathbf{c}_h^{\text{T}}\hat{\mathbf{x}}_h \tag{30}$$

  with $\hat{\mathbf{x}}_h(0) = \hat{\mathbf{x}}_{h,0}$.
- *parameter estimator* which provides the adaptive estimates of $\hat{\omega}_h$, $\hat{\boldsymbol{\theta}}_h$, and $\hat{\sigma}_h$ according to

$$\dot{\hat{\boldsymbol{\theta}}}_h = \Gamma_h \text{Proj} \left(\hat{\boldsymbol{\theta}}_h, -\tilde{\mathbf{x}}_h \mathbf{P}_h \mathbf{b}_h \mathbf{x}_h \right), \ \hat{\theta}_h(0) = \hat{\theta}_{h,0} \tag{31}$$

$$\dot{\hat{\sigma}}_h = \Gamma_h \text{Proj} \left(\hat{\sigma}_h, -\tilde{\mathbf{x}}_h \mathbf{P}_h \mathbf{b}_h \right), \ \hat{\sigma}_h(0) = \hat{\sigma}_{h,0} \tag{32}$$

$$\dot{\hat{\omega}}_h = \Gamma_h \text{Proj} \left(\hat{\omega}_h, -\tilde{\mathbf{x}}_h \mathbf{P}_h \mathbf{b}_h \delta \right), \ \hat{\omega}_h(0) = \hat{\omega}_{h,0} \tag{33}$$

  where $\tilde{\mathbf{x}}_h = \hat{\mathbf{x}}_h - \mathbf{x}_h$; $\Gamma_h \in \mathbb{R}^+$ is the adaptation gain, and $\mathbf{P}_h = \mathbf{P}_h^{\text{T}} > 0$ is the solution of the Lyapunov equation $\mathbf{A}_{m,h}^{\text{T}}\mathbf{P}_h + \mathbf{P}_h\mathbf{A}_{m,h} = -\mathbf{Q}_h$ for an arbitrary $\mathbf{Q}_h = \mathbf{Q}_h^{\text{T}} > 0$.
- *controller* which commands the deflection δ of the waterjet engine according to

$$\delta(s) = -k_h D_h(s) \left(\hat{\eta}_h(s) - k_{g,h}\psi_{\text{ref}}(s) \right) \tag{34}$$

  where $\hat{\eta}_h(s)$ and $\psi_{\text{ref}}(s)$ are the Laplace transforms of $\hat{\eta}_h = \hat{\omega}_h \delta + \hat{\boldsymbol{\theta}}_h \mathbf{x}_h + \hat{\sigma}_h$ and of the reference heading angle, respectively. Setting the filter $D_h(s) = 1/s$ yields the low-pass filter $C_h(s) = \frac{\omega_h k_h}{s + \omega_h k_h}$, whose cutoff frequency is determined by the controller gain k_h. The feedforward gain $k_{g,h} = -1/(\mathbf{c}_h^{\text{T}}\mathbf{A}_{m,h}^{-1}\mathbf{b}_h)$ guarantees reference tracking and zero steady state error for step changes of ψ_{ref}.

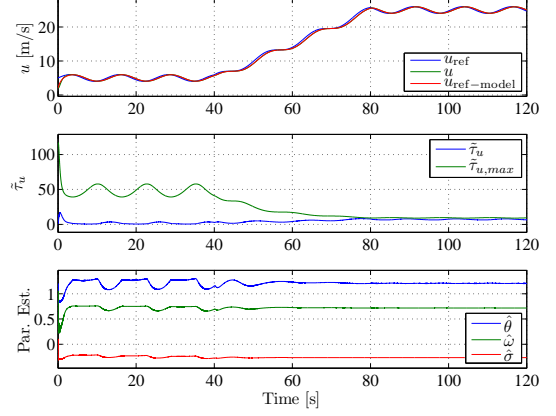*Design Specification*   The closed loop steering dynamics is designed in order to have a damping factor of 0.7 and a

Fig. 9. $\mathcal{L}_1$ cruise controller: reference tracking performance.

95% settling time $t_{s,95} \approx 3\,\text{s}$. These specifications resolve into the following system matrix

$$\mathbf{A}_{m,h} = \begin{bmatrix} 0 & -1 \\ 1 & -1.4 \end{bmatrix} \tag{35}$$

In order to guarantee robustness of the closed loop system the $\mathcal{L}_1$-norm condition (Hovakimyan and Cao, 2010) must be satisfied

$$\|G_h(s)\|_{\mathcal{L}_1}L_h < 1 \tag{36}$$

where

$$G_h(s) = H_h(s)(1 - C_h(s))$$
$$H_h(s) = (s\mathbf{I} - \mathbf{A}_{m,h})^{-1}\mathbf{b}_h$$
$$L_h = \max_{\boldsymbol{\theta_h} \in \Theta_h} \|\boldsymbol{\theta}\|_1$$

Figure 8 (bottom plot) shows a numerical evaluation of condition (36) for increasing value of the filter bandwidth k. It is seen that the $\mathcal{L}_1$-norm condition is satisfied for $k > 60$. A slightly larger bandwidth was chosen using $k = 80$; furthermore the adaptation gain Γ_h was set to 10^5.

5. SIMULATION RESULTS

5.1 Cruise Control Performance Analysis

Figure 9 shows the performance of the $\mathcal{L}_1$ adaptive cruise controller in tracking a reference speed of the form

$$u_{\text{ref}} = U_0 + A_u \sin(2\pi f_u t) + U_1(t - t_r) \tag{37}$$

where t_r is the start time of the ramp. It can be observed that although the nonlinear surge dynamics is completely unknown the surge speed tracks the reference well.

Fig. 10 shows the $\mathcal{L}_1$ adaptive cruise controller tested over the entire range of speeds of the PWC. The reference is a staircase, starting at 2 m/s and increasing with 5 m/s every 10 seconds. Note that the first four steps show very similar performance, whereas for the last reference step, from 22 m/s to 27 m/s, the rise time significantly increases. This relates to the saturation of the thrust commanded, which is not present during the first steps.
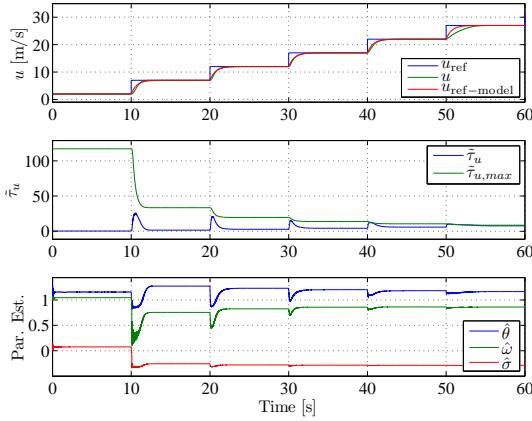
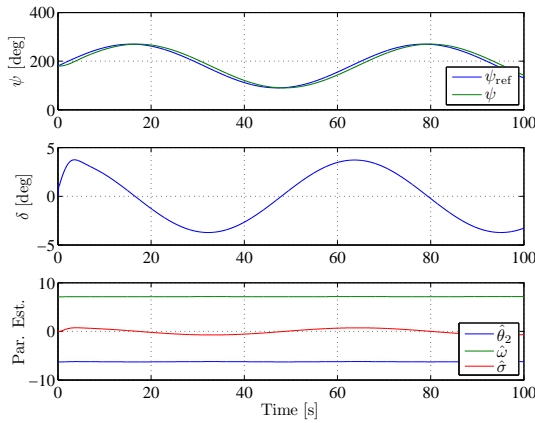Fig. 10. $\mathcal{L}_1$ cruise controller: staircase speed changes.

Fig. 11. $\mathcal{L}_1$ steering, sine curve as reference

5.2 Steering Control Performance Analysis

The performance of the $\mathcal{L}_1$ adaptive steering control was tested by tracking a sinusoidal reference, as shown in Fig. 11. It is seen that the system is able to follow the reference well.

6. CONCLUSION

This paper has suggested and identified a simplified 4DOF manoeuvring model for a high-speed personal water craft. Grey-box identification was performed by exploiting several data sets from full scale sea trials, including spiral and zig-zag tests. The identification clearly pointed out the dependence of the manoeuvring characteristics on the running attitude of the vehicle. This emphasised the necessity of designing an adaptive autopilot, which could guarantee equal performance through the entire range of operational conditions.

By exploiting the knowledge about parameters' variations gathered through the identification procedure, an adaptive manoeuvring controller was designed by means of $\mathcal{L}_1$ adaptive control theory (Hovakimyan and Cao, 2010). The $\mathcal{L}_1$ adaptive autopilot was shown to guarantee both robustness and stability of the closed loop system in different operational conditions. Simulations showed promise of convincing performance.

Subsequent full scale implementation and testing confirmed the expectations but for reasons of space it was not possible to include these very latest results here.

REFERENCES

Blanke, M. (1981). *Ship Propulsion Losses Related to Automated Steering and Prime Mover Control*. Ph.D. thesis, Technical University of Denmark.

Blanke, M. and Christensen, A. (1993). Rudder-roll damping autopilot robustness due to sway-yaw-roll couplings. In *Proceedings of the 10th International Ship Control System Symposium*.

Blanke, M., Lindegaard, K.P., and Fossen, T.I. (2000). Dynamic model for thrust generation of marine propellers. In *Proceedings of the IFAC Conference on Manoeuvreing of Marine Craft*.

Blount, D.B. and Codega, L.T. (1992). Dynamic stability of planing boats. *Marine Technology*, 29-1, 4–12.

Breu, D.A. and Fossen, T.I. (2011). L1 adaptive and extremum seeking control applied to roll parametric resonance in ships. In *Proc. IEEE International Conference on Control & Automation (ICCA)*.

Clarke, D. and Horn, J.R. (1997). Estimation of hydrodynamic derivatives. In *Proceedings of the 11th Ship Control Systems Symposium*, volume 2.

Dand, I. (1996). Directional instability and safety of high speed marine vehicles. In *Proceedings of the 5th International Conference on High Speed Marine Craft Safe Design and Safe Operation*.

Fossen, T.I. (1991). *Nonlinear Modeling and Control of Underwater Vehicles*. Ph.D. thesis, Norwegian University of Science and Technology.

Fossen, T.I. (2011). *Handbook of Marine Craft Hydrodynamics and Motion Control*. Wiley-Blackwell.

Hovakimyan, N. and Cao, C. (2010). *L1 Adaptive Control Theory: Guaranteed Robustness with Fast Adaptation*. SIAM Society for Industrial and Applied Mathematics.

Ikeda, Y., Katayama, T., and Okumura, H. (2000). Characteristics of hydrodynamic derivatives in maneuvering equations for super high-speed planing hulls. In *Proceedings of the 10th International Offshore and Polar Engineering Conference*, volume 40, 434–444.

Ljung, L. (1999). *System Identification: Theory for the User*. Prentice Hall, second edition.

Nomoto, K., Taguchi, T., Honda, K., and Hirano, S. (1957). On the steering qualities of ships. *International Shipbuilding Progress*, 4, 354–370.

Perez, T. and Blanke, M. (2012). Ship roll motion control. *Annual Reviews in Control*, 36 (1), 129–147. doi: 10.1016/j.arcontrol.2012.03.010.

Ross, A. (2008). *Nonlinear Manoeuvring Models for Ships: a Lagrangian Approach*. Ph.D. thesis, Norwegian University of Science and Technology.

Son, K.H. and Nomoto, K. (1982). On the coupled motion of steering and rolling of a high speed containership. *Naval Architecture and Ocean Engineering*, 20, 73–83.